J Mater Sci: Mater Electron (2023) 34:1514

Structural, magnetic, and magnetocaloric properties of $La_{0.8-x}Eu_xCa_{0.1}Sr_{0.1}MnO_3$ (x = 0.05, 0.10, and 0.15): A-site doping

Zhuojia Xie[1], Xinyu Jiang[1], Weijian Zhang[1], and Zhengguang Zou[1,2,*]

[1] College of Materials Science and Engineering, Guilin University of Technology, Guilin 541004, China
[2] Collaborative Innovation Center for Exploration of Hidden Nonferrous Metal Deposits and Development of New Materials, Guilin University of Technology, Guilin 541004, China

Received: 5 March 2023
Accepted: 4 July 2023
Published online: 13 July 2023

ABSTRACT

With the development of the current times, the demand for refrigeration is in every aspect. Nevertheless, the necessity for new refrigeration materials is immediate because of the greenhouse effect and the destruction of the atmosphere. Therefore, perovskite materials have been investigated. $La_{0.8-x}Eu_xCa_{0.1}Sr_{0.1}MnO_3$ (LECSMO) (x = 0.05, 0.10, 0.15) powder samples were prepared using the sol–gel method (S–G). The structure, magnetocaloric effect, and magnetic of LECSMO have been explored. X-ray diffraction (XRD) indicates that all samples belong to the rhombohedral perovskite structure of the Pbnm space group. The magnetic research of LECSMO revealed that the samples doped with Eu^{3+} exhibited a ferromagnetic (FM) to paramagnetic (PM) transition around the Curie temperature (Tc). As the amount of Eu^{3+} doping is added, Tc decreased from 264 to 194 K. Normalization and Banerjee's criterion confirmed the second-order phase transition of the LECSMO near Tc. The maximum magnetic entropy change ($-\Delta S_M^{max}$) for LECSMO (x = 0.05, 0.10, 0.15) is 5.39, 4.52, and 4.35 J/(kg·K) when the applied magnetic field (H) = 5 T, respectively. Further, the relative cooling power (RCP) of LECSMO is 282.20 $J \cdot kg^{-1}$, 305.20 $J \cdot kg^{-1}$, and 323.15 $J \cdot kg^{-1}$, respectively.

1 Introduction

At present, refrigeration technology has a critical position and is closely related to the production and life of people. Refrigeration technology is used everywhere, for example, in medical equipment, refrigerators, the chemical and petroleum industry, the power industry, and precision instruments [1–5]. In daily life, the commonly used method is gas compression refrigeration. The extensive use of gas

Zhuojia Xie and Xinyu Jiang have contributed equally to this work.

Address correspondence to E-mail: zouzgglut@163.com

https://doi.org/10.1007/s10854-023-10943-4

compression refrigeration (Freon) has caused severe damage to the environment. Therefore, it is vital to find newer cooling methods to achieve better cooling. Under these conditions, magnetic refrigeration technology was created. Since the physical properties of the magnetocaloric effect (MCE), magnetic refrigeration using MCE is becoming increasingly advantageous [6]. Magnetic refrigeration offers better cooling efficiency than conventional gas compression refrigeration and does not cause environmental pollution, making it greener and more energy efficient [7, 8]. The MCE is caused by the magnetized material's demagnetization, cooling, or heating. Whereas, the MCE results from the coupling between the atomic lattice and the magnetic moment, the change in magnetic entropy of magnetic refrigeration materials in the presence of H. The change in entropy for isothermal processes and the change in temperature (T) for adiabatic processes are the basic indicators of performance [9–12]. As a result, researchers have developed new refrigeration materials with a wide operating temperature range and a considerable variation in magnetic entropy change (ΔS_M).

There are hundreds of MCE materials that have been discovered since the 21st century. Metal Gd and Gd-based alloys, $La(FeSi)_{13}$, and $Gd_5Si_2Ge_2$ all exhibit excellent MCE [13–15]. However, these materials are difficult to apply due to their high price, cumbersome synthesis methods, and bigger thermal hysteresis. ABO_3 has attracted much attention and has been extensively investigated because of its low price, simple synthesis route, small magnetic hysteresis and

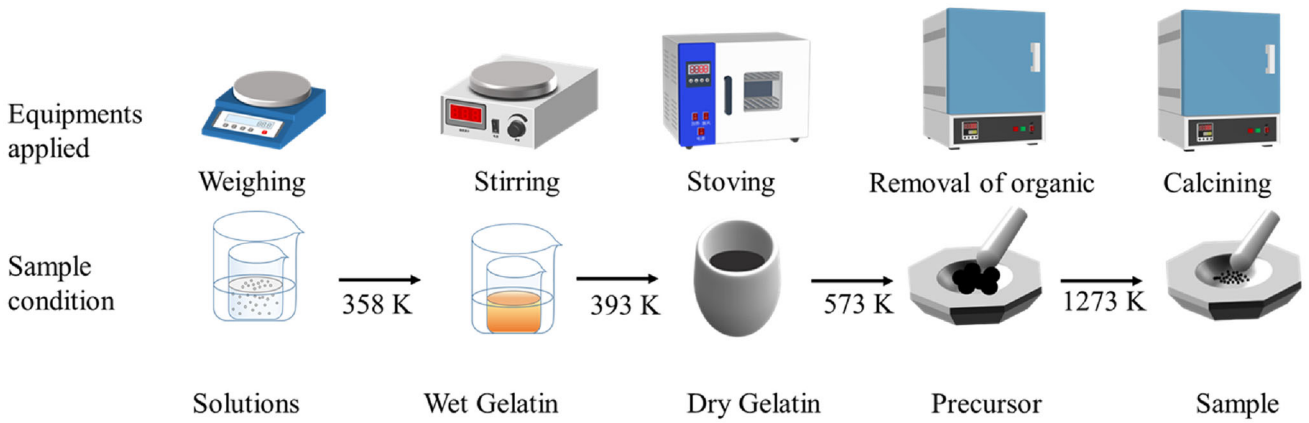

Fig. 1 A flowchart for the preparation of $La_{0.8-x}Eu_xCa_{0.1}Sr_{0.1}MnO_3$ (x = 0.05, 0.10, 0.15)

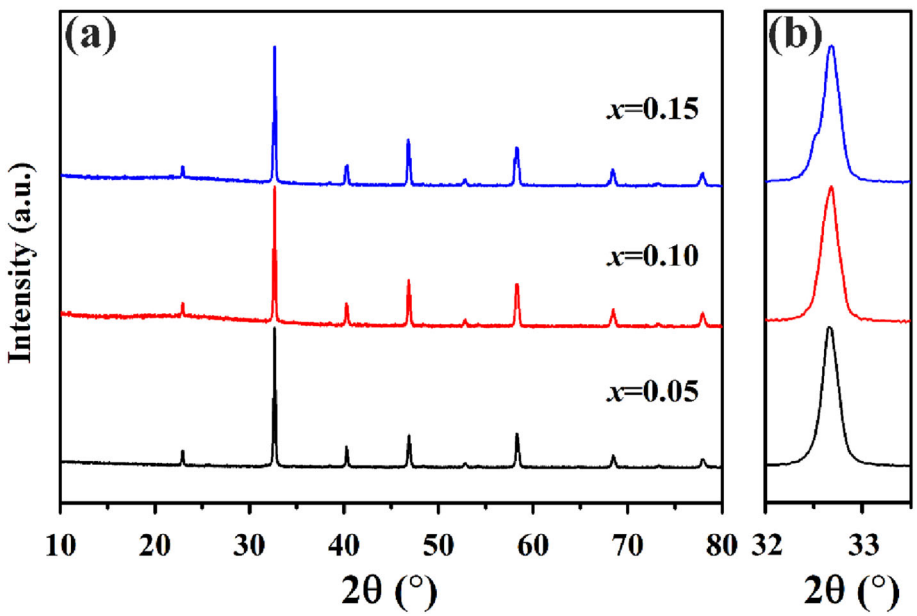

Fig. 2 The XRD patterns of the $La_{0.8-x}Eu_xCa_{0.1}Sr_{0.1}MnO_3$ (x = 0.05, 0.10, 0.15) samples

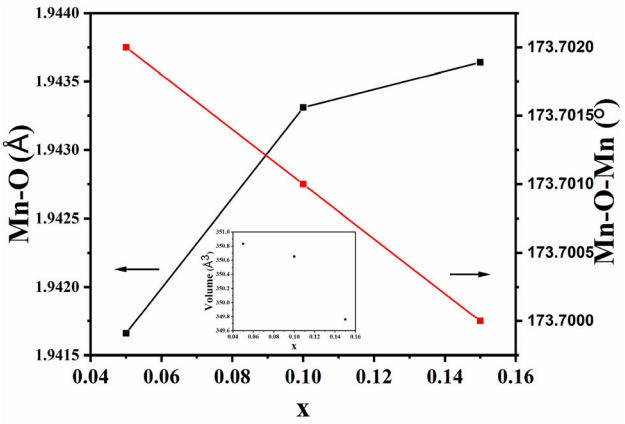

Fig. 3 Changes in Volumes, Mn–O bond length, and Mn–O–Mn bond angle of $La_{0.8-x}Eu_xCa_{0.1}Sr_{0.1}MnO_3$ (x = 0.05, 0.10, 0.15) samples

Table 1 Structural parameters for the LECSMO determined from Rietveld analysis of X-ray powder diffraction data

X	0.05	0.10	0.15
Space group	Pbnm	Pbnm	Pbnm
a (Å)	5.50399	5.50358	5.49952
b (Å)	5.50711	5.50672	5.50262
c (Å)	7.74851	7.74812	7.74403
V (Å^3)	234.870	234.820	234.350
Mn–O (Å)	1.94166	1.94331	1.94364
Mn–O–Mn (°)	173.702	173.701	173.700
R_p (%)	2.31	2.33	2.14
R_{wp} (%)	2.98	3.19	3.02
χ^2	3.542	3.549	3.457
W × 10^2 (a.u.)	9.80378	9.77468	9.76887

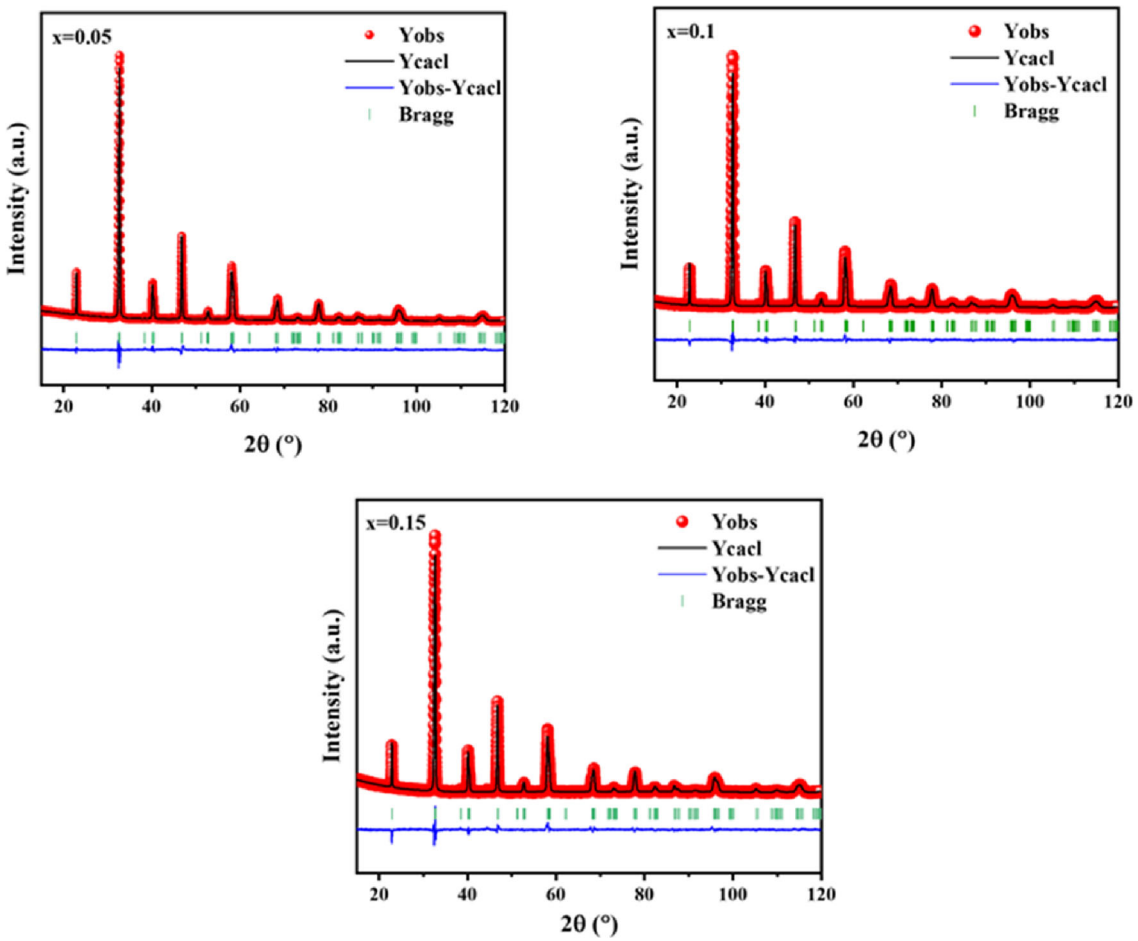

Fig. 4 Rietveld refinement for the $La_{0.8-x}Eu_xCa_{0.1}Sr_{0.1}MnO_3$ (x = 0.05, 0.10, 0.15) samples

thermal hysteresis, and significant ΔS_M [16–19]. Recently, researchers have become very interested in studying $RE_{1-x}AE_xMnO_3$ (RE = La, Pr, Nd, and Sm and AE = Ba, Sr, and Ca) in ABO_3. Because the Tc of $La_{1-x}Sr_xMnO_3$ is suitable and thus could be a potential magnetic refrigeration material [20–23]. Szewczyk et al. found that with Sr^{2+} doping increased, Tc approached near room temperature. When H = 7 T, Tc = 305 K, $-\Delta S_M^{max}$=7.90 J/(kg·K), and RCP=395 J·kg^{-1} [24]. A. Elghoul et al. study given Tc = 330 K for $La_{0.8}Sr_{0.2}MnO_3$ when H = 2 T, $-\Delta S_M^{max}$=1.99 J/(kg·K), RCP=69.07 J·kg^{-1} [17]. When doped with trace amounts of alkaline earth ions (Ca^{2+}, Ba^{2+}), the MCE of ABO_3 can be significantly augmented without affecting the double-exchange interaction (DE) [10, 25, 26].

In order to investigate a refrigeration material with simple preparation, low cost, and axenic, the structural, magnetic, and magnetocaloric properties of LECSMO (x = 0.05, 0.10, 0.15), which the amount of Eu^{3+} doping increases, using $La_{0.8}Ca_{0.1}Sr_{0.1}MnO_3$ as a substrate have been deeply explored.

2 Experimental

In this paper, samples of LECSMO polycrystalline powder were prepared using the S–G method. The amount required for each sample was first calculated from the stoichiometric ratios. ($La(NO_3)_3{\cdot}6H_2O$ 10277-43-7, $Ca(NO_3)_2{\cdot}4H_2O$ 13477-34-4, Sr $(NO_3)_2$ 10042-76-9, $Eu(NO_3)_3{\cdot}6H_2O$ 10031-53-5, and $Mn(NO3)_2$ (50%) 10377-66-9. All chemicals used were of the Aladdin brand and were ≥ 99.5% pure). The gel was then stirred uniformly in a constant temperature water bath at 85 °C until a wet gel was formed. The wet gel was dried at 120 °C for 12 h to obtain a dry gel. The resulting dry gel was subjected to a heat treatment at 300 °C in a muffle furnace to remove the organic matter from the samples. The powder was allowed to cool naturally and then ground. The ground powder was then calcined in a muffle furnace at 950 °C for 10 h to obtain LECSMO polycrystalline powder. (Fig. 1)

XRD with Cu Kα radiation (λ = 1.54059Å) was used to determine the physical phase, structure, and cell parameters of LECSMO. The data were further processed by the Rietveld method. The characteristics of morphology and size of the samples were analyzed

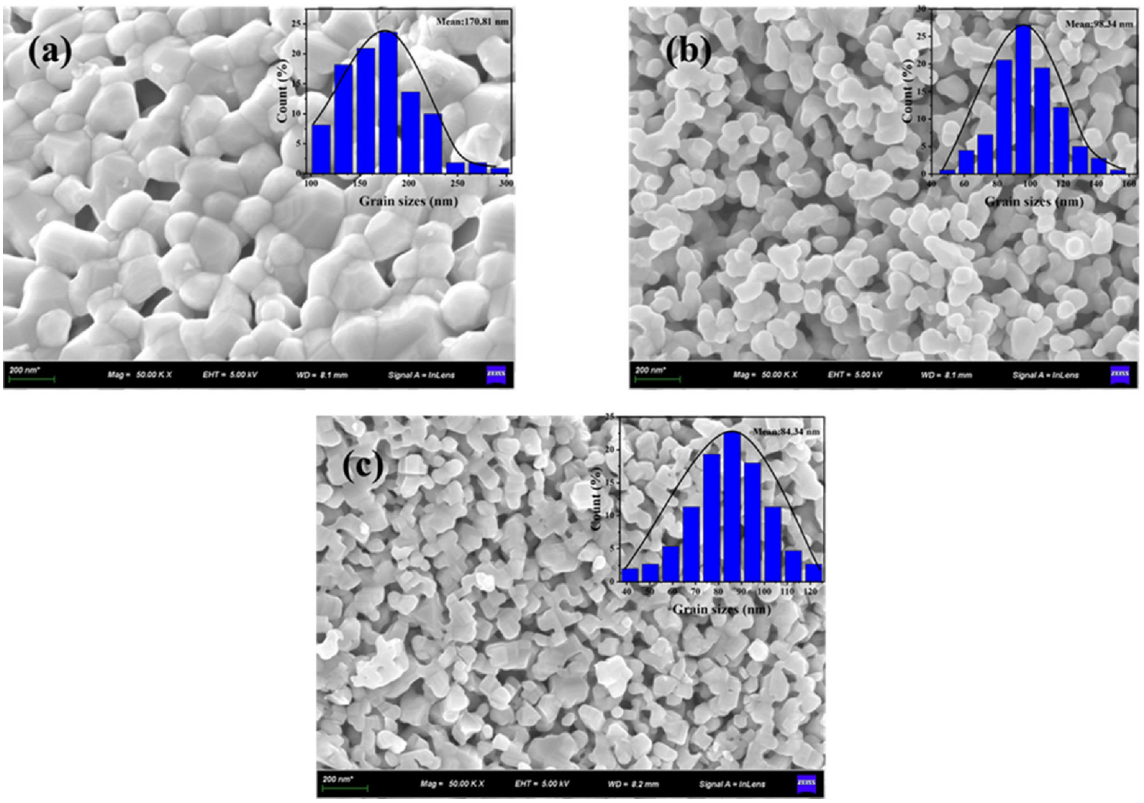

Fig. 5 The scanning electron microscope images and grading curve of $La_{0.8-x}Eu_xCa_{0.1}Sr_{0.1}MnO_3$ (x = 0.05, 0.10, 0.15)

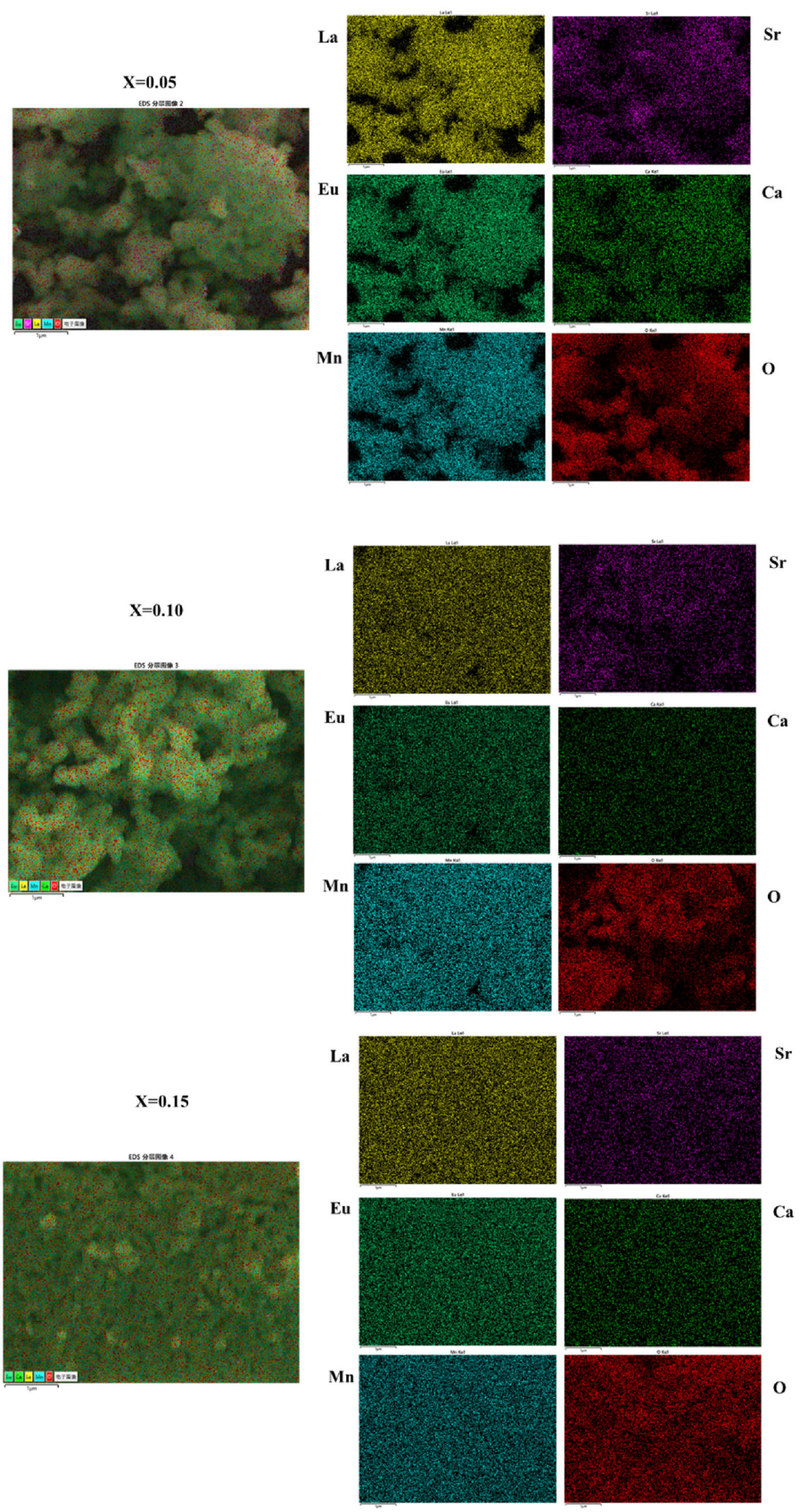

Fig. 6 Scanning electron microscope mapping of $La_{0.8-x}Eu_xCa_{0.1}Sr_{0.1}MnO_3$ (x = 0.05, 0.10, 0.15)

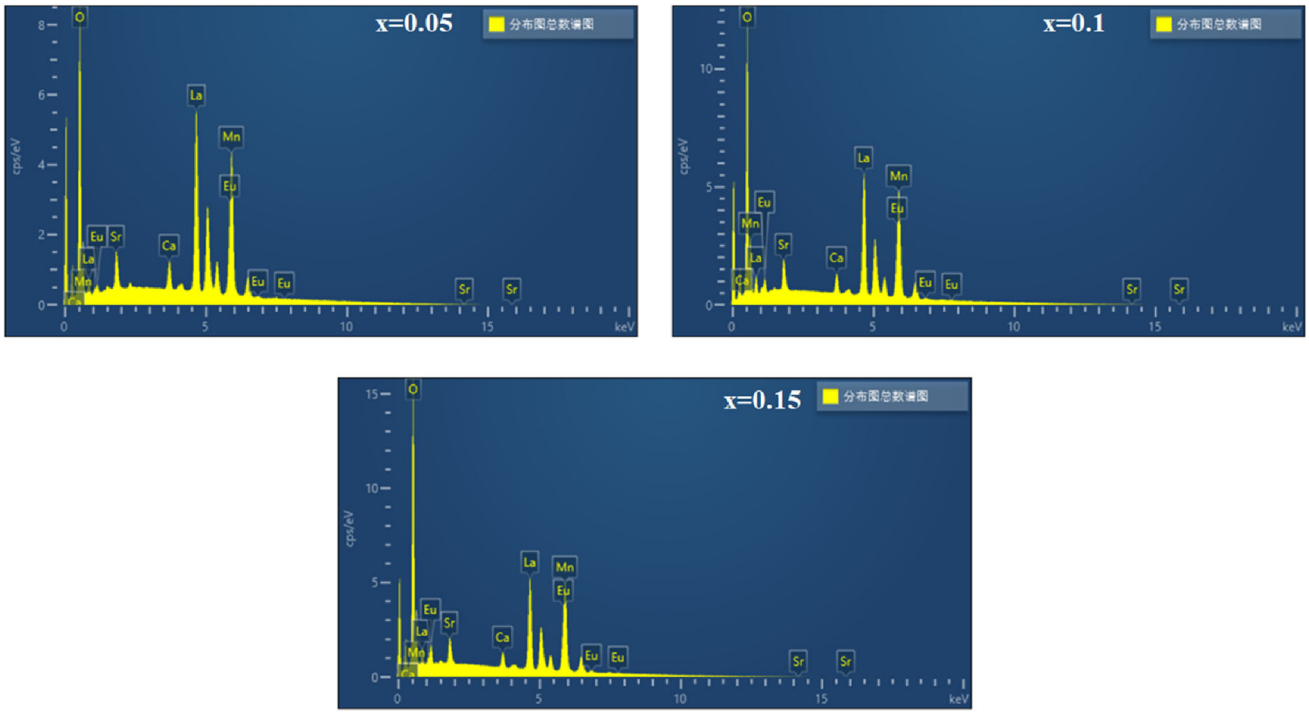

Fig. 7 The energy-dispersive spectrometer results of $La_{0.8-x}Eu_xCa_{0.1}Sr_{0.1}MnO_3$ (x = 0.05, 0.10, 0.15)

by scanning electron microscopy (SEM) (SEM, ZEISS, GeminiSEM 300). Finally, the LECSMO was magnetically tested using the integrated magnetic measurement system MPMS (Quantum Design (USA)).

3 Results and discussion

3.1 Structural exploration

The XRD data of LECSMO at room temperature are shown in Fig. 2. Figure 2 confirms that the LECSMO are all single-phase perovskite and that no impurity phases are detected. Figure 2b is an enlarged figure of the characteristic diffraction peak of the LECSMO diffraction angle of 32–33.5°. The characteristic diffraction peak of LECSMO between 32° and 33.5° shifts slightly toward higher angles with increasing Eu^{3+} content, indicating that the cell volume (V) of samples is diminished. This is because the ionic radius of Eu^{3+} (1.15 Å) is smaller than La^{3+} (1.36 Å). When the smaller ionic radius of Eu^{3+} replaces the larger ionic radius of La^{3+}, the average radius of the A-site ion decreases and therefore V decreases accordingly [27–30]. At the same time, the Mn–O bond length becomes larger, and the Mn–O–Mn bond angle decreases, resulting in a distortion of the LECSMO lattice. Figure 3 demonstrates how the cultural parameters vary with the amount of Eu^{3+} doping. Refinement of the XRD data from LECSMO by FULLPROF software confirmed that LECSMO is a rhombohedral perovskite structure with a Pbnm space group (Fig. 4).

Table 1 displays the calculated lattice constants, V, Mn–O–Mn bond angles, and Mn–O bond lengths and summarizes the fit χ^2 for LECSMO. To determine the degree of stability of the LECSMO architecture, the tolerance factor (t) Goldschmidt introduced is defined [31]. The equation is as follows:

$$t = \frac{(r_A + r_O)}{\sqrt{2}(r_B + r_O)}. \quad (1)$$

r_O, r_B, and r_A are the average ionic radii at the O, B, and A positions in the LECSMO perovskite manganites, respectively. The average LECSMO ion radius size was calculated using the Shannon table and Eq. (1). The calculated t for LECSMO is less than 0.96, confirming that it is a stable rhombohedral perovskite structure. The bandwidth W is decided from the angle of Mn–O–Mn and the length of Mn–O, which is calculated as follows [32]:

$$W = \frac{cos\frac{(\pi - <Mn-O-Mn>)}{2}}{(<Mn-O>^{3.5})}. \quad (2)$$

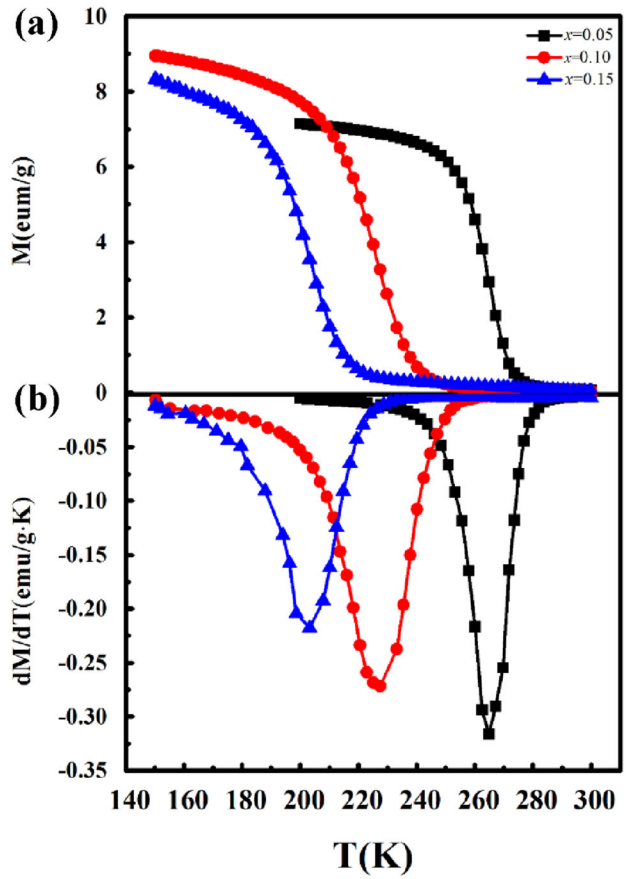

Fig. 8 Magnetization (100 Oe) vs. Temperature curve and dM/dT vs. Temperature curve for $La_{0.8-x}Eu_xCa_{0.1}Sr_{0.1}MnO_3$ (x = 0.05, 0.10, 0.15)

Table 1 presents that as the amount of Eu^{3+} doping augments, the Mn–O–Mn bond angle declines, while the Mn–O bond length increases, leading to a decrease in W. The decrease in W reduces the overlap between the Mn 3d orbital and the 2p orbital of the O anion, reducing the Mn^{4+}–O^{2-}–Mn^{3+} exchange coupling and weakening the DE interaction, ultimately weakening, leading to a decrease in Tc.

Figure 5 manifests the SEM diagram of LECSMO. The particles of LECSMO show an irregular elliptical distribution with porosity. LECSMO is available in sub-micron crystalline size spanning from 84 to 171 nm. The average crystalline size (D_{XRD}) of LECSMO can be obtained according to Scherrer's formula [33]

$$D_{XRD} = \frac{K\lambda}{\beta\cos(\theta)}. \quad (3)$$

K is the Scherrer constant, λ is the wavelength of the x-rays, θ is the Bragg diffraction angle, and β is the half-height width of the LECSMO diffraction peak. The D_{XRD} range of LECSMO is between 50 and 100 nm. Results show that the size of the LECSMO particles viewed by SEM is bigger than the D_{XRD} obtained by the Scherrer equation since each particle in LECSMO is made up of multiple grains [10, 17, 34].

Table 2 The values of Tc, θ_w (C-W temperature), C (Curie constant), μ_{eff}^{exp}, and μ_{eff}^{the}

X	0.05	0.10
Tc (K)	264	226
θ_w (K)	269	237
C (u_B.K/T)	4.70	6.44
$\mu_{eff}^{exp}(\mu_B)$	6.13	7.18
$\mu_{eff}^{the}(\mu_B)$	4.58	4.45

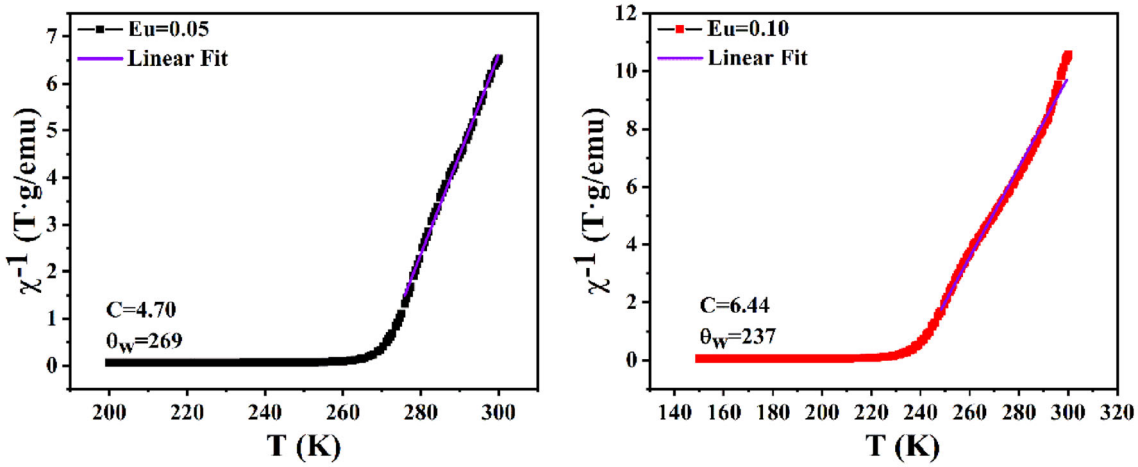

Fig. 9 Inverse susceptibility vs. Temperature curves generated for $La_{0.8-x}Eu_xCa_{0.1}Sr_{0.1}MnO_3$ (x = 0.05, 0.10, 0.15) at H = 100 Oe

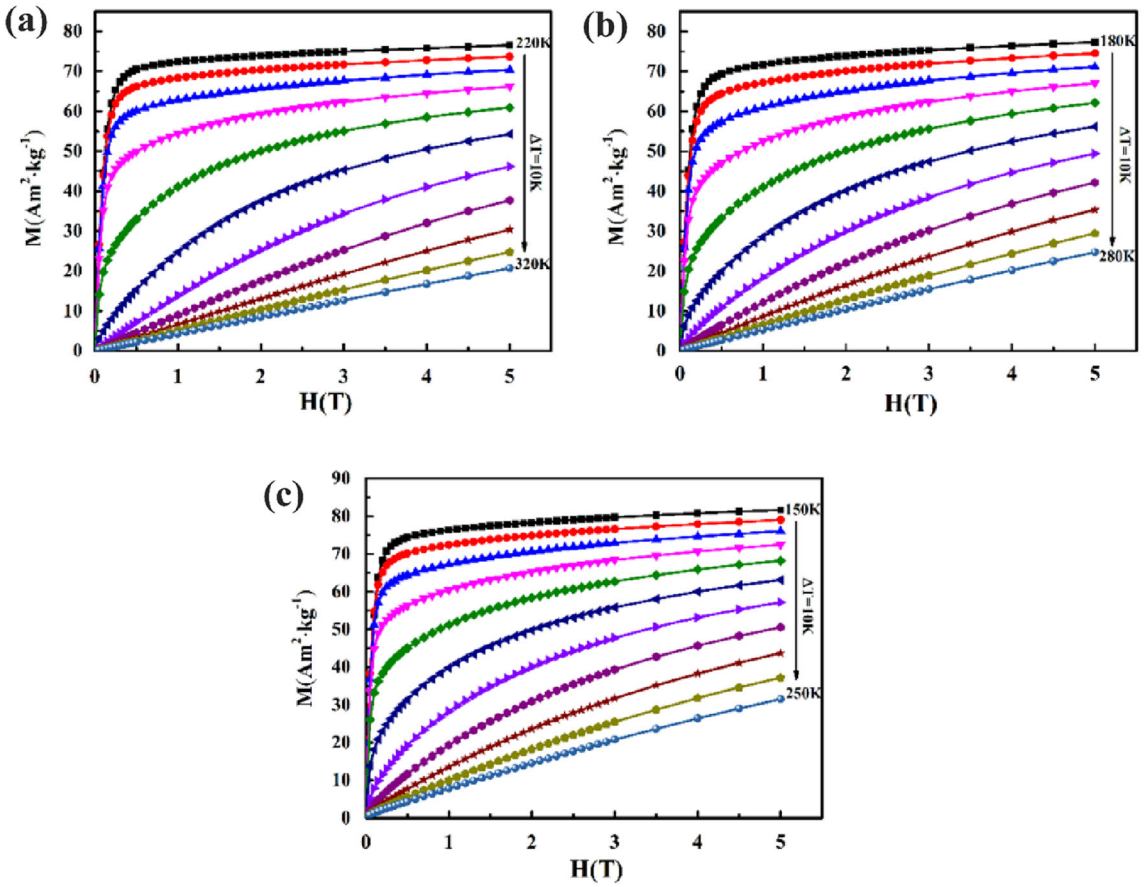

Fig. 10 Isothermal magnetization for $La_{0.8-x}Eu_xCa_{0.1}Sr_{0.1}MnO_3$ (x = 0.05, 0.10, 0.15)

Figure 6 indicates the scanning electron microscope mapping of $La_{0.8-x}Eu_xCa_{0.1}Sr_{0.1}MnO_3$ (x = 0.05, 0.10, 0.15). Verification of the presence of all elements in LECSMO by energy-dispersive spectrometer analysis (Fig. 7). Energy-dispersive spectrometer analysis confirmed the existence of La, Ca, Mn, Eu, Sr, and O elements in the LECSMO.

3.2 Magnetic and Magnetocaloric Exploration

LECSMO is magnetized in the temperature (T) scale of 140−300 K in a field of 100 Oe. As shown in Fig. 8, with T increased, the magnetization intensity (M) of LECSMO diminished sharply. They indicated an FM-PM transition of the polycrystalline powder LECSMO. Tc is determined by differentiating the M–T curve, and the smallest value of Tc corresponding to dM/dT is determined as a consequence of T. (Fig. 8). Figure 8 presents Tc for different Eu^{3+} doping amounts are 264, 226, and 194 K. The variation of Tc is related to the DE within the LECSMO material. As the radius of Eu^{3+} is smaller than that of La^{3+}, as the amount of Eu^{3+} doping increased, the r_A decreased, distorting the lattice of LECSMO. The degree of lattice distortion can be expressed in the magnitude of the mismatch coefficient (σ^2), which is defined as follows [35]

$$\sigma^2 = <r_A{}^2> - <r_A>^2. \quad (4)$$

Equation (4) calculates the σ^2 for LECSMO (x = 0.05, 0.10, 0.15) as 0.6944, 0.7908, and 0.8715, respectively. The increase in σ^2 with Eu^{3+} doping indicates an enhanced disorder and increased distortion of the A-site ions in LECSMO. The distortion leads to a reduction in the Mn–O–Mn bond angle and an enlargement of the Mn–O bond length, affecting Mn^{3+}–O^{2-}–Mn^{4+}, leading to a weakness in DE and a reduction in Tc. Since the Tc of LECSMO (x = 0.05, 0.10) is closer to that required for low to medium room temperature refrigeration, the magnetic behavior of LECSMO (x = 0.05, 0.10) was further

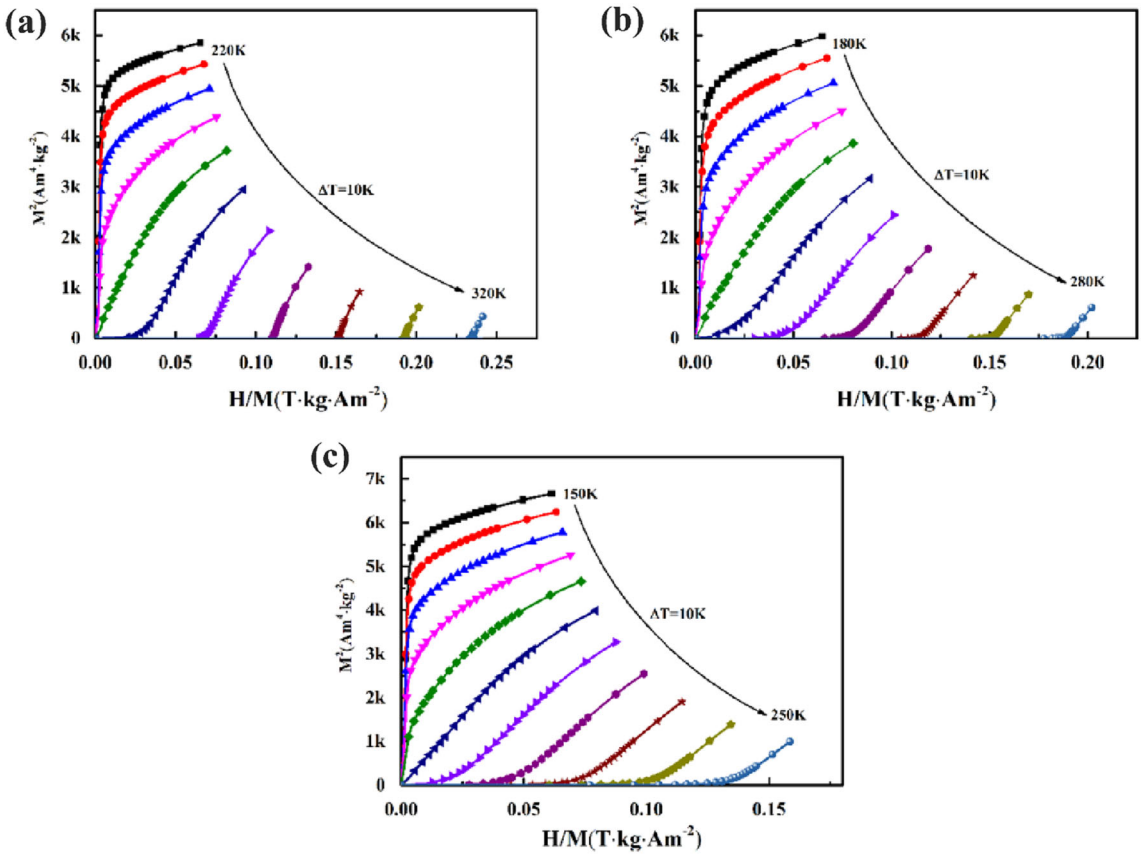

Fig. 11 Arrott plots of magnetization isotherms generated for $La_{0.8-x}Eu_xCa_{0.1}Sr_{0.1}MnO_3$ (x = 0.05, 0.10, 0.15)

investigated in depth using the Curie–Weiss law (C–W) (Fig. 9) [36, 37]:

$$X = \frac{C}{T - \theta_W}. \tag{5}$$

C is the Curie constant and θ_W is the Weiss temperature. The value of c is greater than Tc (Table 2). The differences in θ_W and Tc may have some relevance to the presence of magnetic inhomogeneities. Table 2 shows that θ_W decreases significantly with increasing Eu^{3+} doping, showing a decreased DE, associated with a decreasing Tc. A positive value of θ_W indicates the presence of FM interactions.

C can be determined from C–W and the experimental effective magnetic moment μ_{eff}^{exp} is defined by equation [38]:

$$C = \frac{N_A \mu_B^2}{3K_B} \times \mu_{eff}^{exp2}. \tag{6}$$

N_A is the Avogadro constant, μ_B is the Bohr magneton, and K_B is the Boltzmann constant. The following relation can determine the theoretical effective magnetic moment μ_{eff}^{the} [39]:

$$\mu_{eff}^{the} = \sqrt{(0.8 - x)u_{eff}^2(Mn^{3+}) + 0.2u_{eff}^2(Mn^{4+})}. \tag{7}$$

μ_{eff}^{the} and μ_{eff}^{exp} are shown in Table 2. μ_{eff}^{exp} gradually raised as the amount of Eu^{3+} doping was added. The change in μ_{eff}^{exp} is the opposite of the change in Tc. The variance can illustrate the phenomenon in the strength limit of the FM association between Mn^{3+} and Mn^{4+}. μ_{eff}^{exp} for the LECSMO (x = 0.05, 0.10) samples are more remarkable than μ_{eff}^{the}, also confirming the presence of FM interactions in the PM phase. The difference in the strength limit of the FM interaction between Mn^{3+} and Mn^{4+} can illustrate this phenomenon. LECSMO (x = 0.05, 0.10) samples with μ_{eff}^{exp} greater than μ_{eff}^{the} confirmed the presence of FM interactions in the PM phase. Figure 10 shows the isothermal magnetization profiles (M–H) of LECSMO at different T. The range of H is 0–5 T, with a curve measured at 10 K intervals. It was found that the

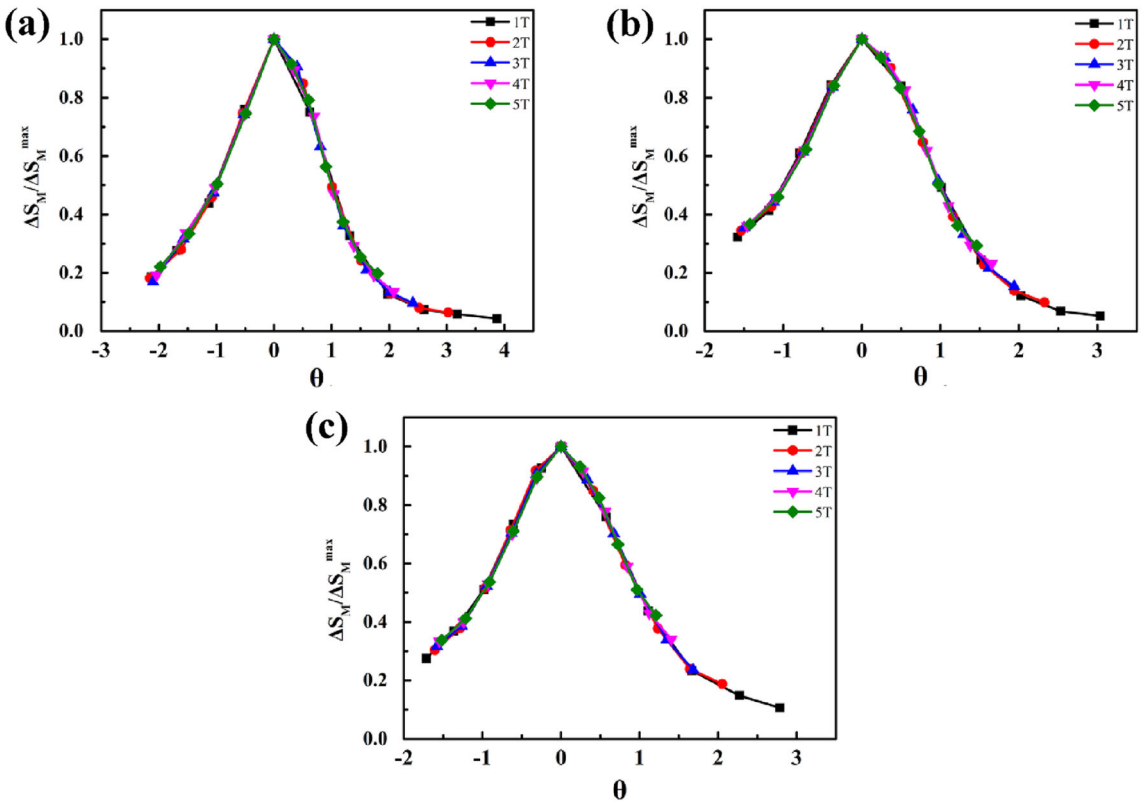

Fig. 12 Universal curves of $La_{0.8-x}Eu_xCa_{0.1}Sr_{0.1}MnO_3$ (x = 0.05, 0.10, 0.15)

maximum M of LECSMO increased from 76.5 Am^2 kg^{-1} (x = 0.05) to 81.6 Am^2 kg^{-1} (x = 0.15) as the Eu^{3+} doping content increased. When T of LECSMO is lower than Tc and H is lower than 0.3 T, M of LECSMO tends to rise rapidly with increasing H. When H is more incredible than 0.3 T, M increases slowly and eventually tends to saturate gradually. When T < Tc, LECSMO has a larger M and exhibits typical FM behavior. When T > Tc, the M of LECSMO is relatively small and exhibits typical PM behavior. At the same H, the higher the T, the smaller the M of the LECSMO, determining that the LECSMO underwent an FM-PM phase transition. Figure 10 demonstrates that M–H is not all linear when T > Tc, explaining the reason for the difference between μ_{eff}^{the} and μ_{eff}^{exp} and demonstrating the presence of FM clusters in PM.

To further investigate the use of magnetic phase transformation in LECSMO, M^2-H/M curves (Arrott curves) were graphed in the critical temperature region of the phase transformation (Fig. 11). The Banerjee criterion allows the type of magnetic phase change of LECSMO to be discerned. In the Arrott curve, if the M^2-H/M curve has a negative slope around Tc or if the curve is S shaped, then the type of magnetic phase transition of the sample is a first-order phase transformation. If the gradient of the M^2-H/M curve around Tc is all positive, then the type of magnetic phase transformation of the material is a second-order phase transformation. The more negligible hysteresis of the second-order phase transition facilitates the practical application of LECSMO magnetically refrigeration materials.

The type of phase transition in LECSMO is determined using the Banerjee criterion and the field-following normalization curve proposed by Franco. The normalization curve assumes that if there is a normalization curve, the curves at various of H collapse into a single curve, and the corresponding phase transition for that material becomes the second-phase transformation. The curve at various H cannot be collapsed into a curve with a primary phase transformation. This is defined by Equations. [40, 41]:

$$\theta = \begin{cases} (Tc - T)/(T_1 - T_c), (T \le TC) \\ (T - Tc)/(T_2 - Tc), (T > TC) \end{cases}. \quad (8)$$

T_1 and T_2 temperatures all need to satisfy $\Delta S_M(T_2) = \Delta S_M(T_1) = \frac{1}{2}\Delta S_M^{Max}$. The normalized curves of LECSMO at various H can all slump into one curve. Confirming that the phase transitions occurring in LECSMO are all second-order phase transitions, in agreement with the results obtained using the Banerjee criterion (Fig. 12).

The ΔS_M of LECSMO is obtained from the adiabatic change of T under a magnetic field. The equation for the ΔS_M is obtained using Maxwell's thermodynamic relations as follows [42]:

$$\Delta S_M(\mathrm{T},\ \mathrm{H_{MAX}}) = S(\mathrm{T},\ \mathrm{H_{MAX}}) - \mathrm{S}(\mathrm{T},0) = \int_0^{\mathrm{H_{MAX}}} \left(\frac{\partial M}{\partial T}\right)_H dH. \quad (9)$$

The magnetization measurements are carried out at discrete magnetic fields and T separation, which can be circa by Eq. (9) as Eq. (10) [43].

$$\Delta S(T,H) = \sum_i \frac{M_{i+1}(T_{i+1},H) - M_i(T_i,H)}{T_{i+1} - T_i}\Delta H, \quad (10)$$

where M_i and M_{i+1} are the experimental magnetization values at T_i and T_{i+1} temperatures, respectively. The relationship between the ΔS_M of LECSMO at different H and T are given in Fig. 13. At the same T, the ΔS_M of LECSMO increases gradually with increasing H. This is because increasing H increases the degree of ferromagnetic long-range ordering in LECSMO, which accelerates the change in M of the sample near Tc and ultimately leads to an increase in the ΔS_M. The $-\Delta S_M^{max}$ of LECSMO is 5.39 J/(kg·K), 4.52 J/(kg·K), and 4.35 J/(kg·K) at H = 5 T. The ΔS_M of LECSMO decreases with increasing x, which is related to the weakening of DE inside the LECSMO sample. As the amount of Eu^{3+} doping increases, the MnO_6 octahedral distortion becomes more and more severe, affecting the DE of Mn^{3+}–O^{2-}–Mn^{4+} and

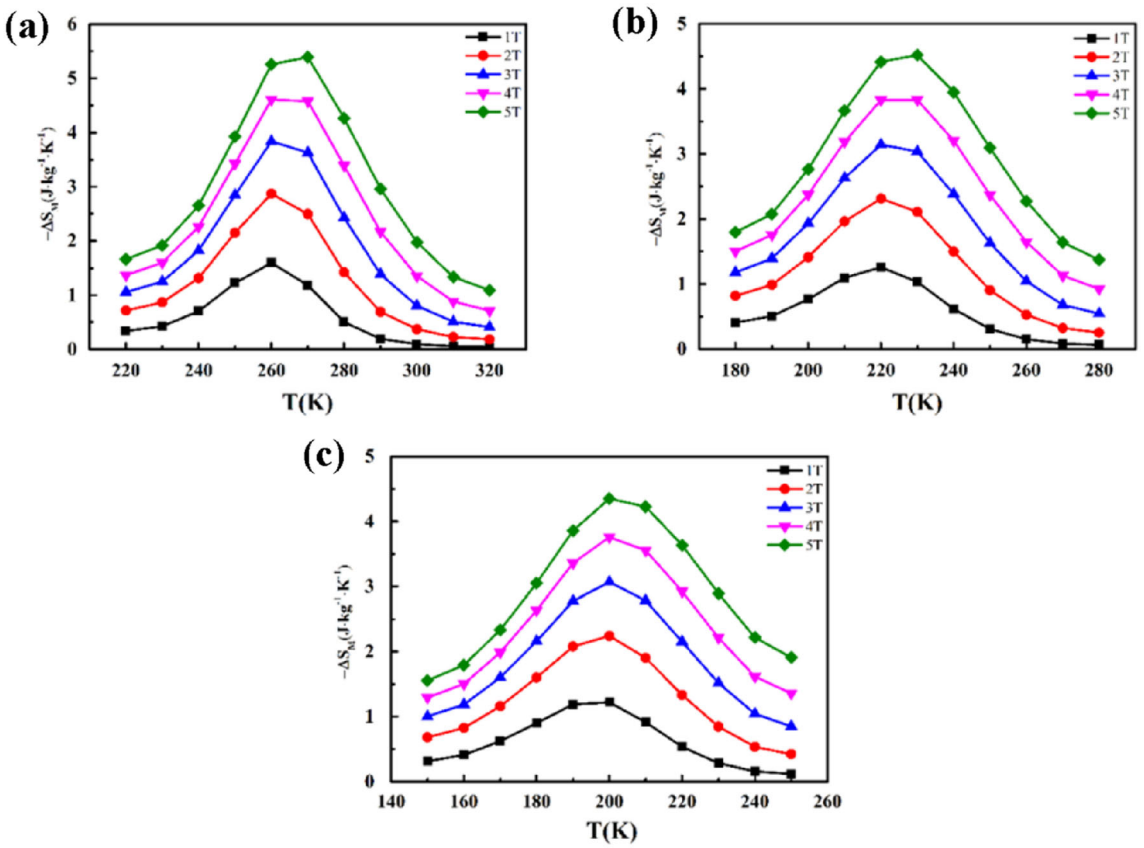

Fig. 13 $-\Delta S_M$ vs. T curves generated for $La_{0.8-x}Eu_xCa_{0.1}Sr_{0.1}MnO_3$ (x = 0.05, 0.10, 0.15) in 1–5 T

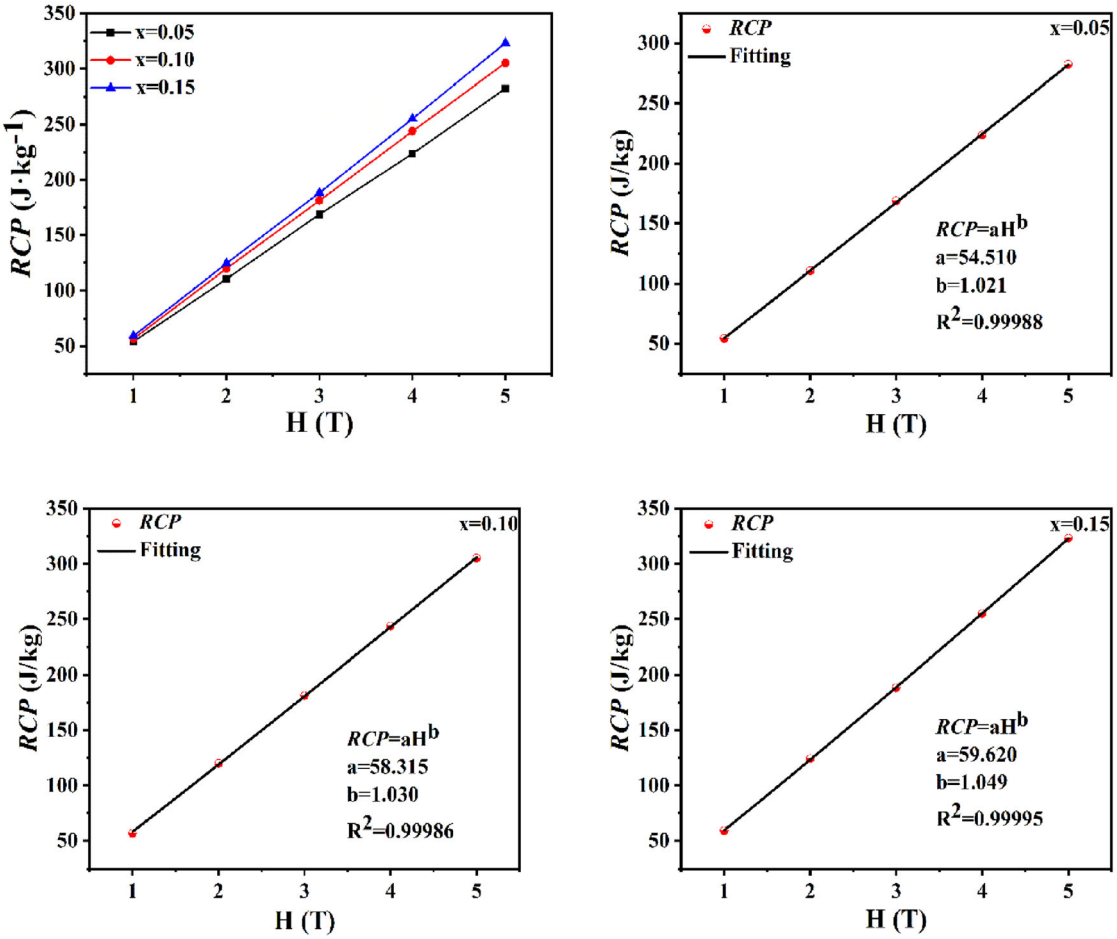

Fig. 14 Relative cooling power as a function of H recorded for the $La_{0.8-x}Eu_xCa_{0.1}Sr_{0.1}MnO_3$ (x = 0.05, 0.10, 0.15). The plot of Relative cooling power as a function of H. The solid line presents the result of the fit conducted when $RCP = aH^b$

eventually leading to a decrease in the $-\Delta S_M^{max}$ variation of LECSMO.

For magnetic refrigeration materials, the relative cooling efficiency (RCP) is an essential parameter for judging their performance, and the RCP is calculated using formula [44]

$$RCP = -\Delta S_M^{max} \times \delta T_{FWHM}, \tag{11}$$

where δT_{FWHM} is the magnitude of the half-peak width of the $-\Delta S_M^{max}$ curve. The RCP of LECSMO varies as a function of H, as shown in Fig. 14 . It can be seen from the graph that the RCP of LECSMO gradually rises as H added. According to the equation $RCP = aH^b$, it is shown that RCP is reliant on H. The b-values obtained after the fit was similar to those previously reported. The RCP for LECSMO was greatest when H = 5 T. The RCP for LECSMO was 282.20 J·kg^{-1} (x = 0.05), 305.20 J·kg^{-1} (x = 0.10), and 323.15 J·kg^{-1} (x = 0.15), respectively. The ΔS_M of LECSMO is gradually enhanced in the RCP as the amount of Eu3 + doping rises, although it is declining. The magnitudes of Tc, $-\Delta S_M^{Max}$, and RCP for LECSMO are listed in Table 3 for comparison with the values for other magnetic materials at H.

According to thermodynamic theory, the variations in magnetic entropy are obtained from the following equation for individual heat capacity.

$$\Delta S_M = \int_0^T \frac{C_P(T,\mu_0 H) - C_P(T,0)}{T} dT. \tag{12}$$

The change in H leads to variations in specific heat (ΔC_p), which can be derived from the following equation [57]:

Table 3 $-\Delta S_M^{max}$, Tc, and *RCP* values of LECSMO and the previously reported manganites

Sample	$H(T)$	$Tc(K)$	$-\Delta S_{Max}(Jkg^{-1}K^{-1})$	$RCP(Jkg^{-1})$	References
$La_{0.75}Eu_{0.05}Ca_{0.1}Sr_{0.1}MnO_3$	2 T	264 K	2.87	110.38	This work
	3 T	264 K	3.84	168.67	This work
	5 T	264 K	5.39	282.20	This work
$La_{0.70}Eu_{0.10}Ca_{0.1}Sr_{0.1}MnO_3$	2 T	226 K	2.31	119.81	This work
	5 T	226 K	4.52	305.20	This work
$La_{0.65}Eu_{0.15}Ca_{0.1}Sr_{0.1}MnO_3$	2 T	194 K	2.24	124.38	This work
	5 T	194 K	4.35	323.15	This work
$La_{0.8}Sr_{0.1}Ca_{0.1}MnO_3$	5 T	280.67	0.52	13.412	[45]
Gd	3 T	294 K	7.10	410.00	[46]
Gd	5T	294 K	10.2	410	[47]
$La_{0.9}Sr_{0.1}MnO_3$	5 T	118 K	2.16	306.59	[48]
$Pr_{0.5}Sr_{0.5}MnO_3$	2 T	268 K	0.82	54.80	[49]
$La_{0.6}Eu_{0.1}Sr_{0.3}MnO_3$	2 T	343 K	1.55	69.00	[50]
$La_{0.75}Sr_{0.1}Ca_{0.15}MnO_3$	2 T	305 K	2.49	78.00	[51]
$La_{0.85}Eu_{0.05}Sr_{0.1}MnO_3$	5 T	121 K	1.95	268.11	[52]
$La_{0.7}Sr_{0.3}Mn_{0.925}Ni_{0.075}O_3$	3 T	256 K	0.81	105.00	[53]
$La_{0.7}Sr_{0.3}Mn_{0.875}Ni_{0.125}O_3$	3 T	180 K	0.71	47.00	[53]
$La_{0.55}Pr_{0.1}Sr_{0.35}Mn_{0.95}Ti_{0.05}O_3$	3 T	288 K	2.78	118.85	[54]
$Pr_{0.75}Bi_{0.05}Sr_{0.1}Ba_{0.1}Mn_{0.96}Ti_{0.04}O_3$	5 T	275 K	3.66	162.00	[55]
$La_{0.6}Bi_{0.1}Sr_{0.15}Ca_{0.15}Mn_{0.9}Cu_{0.1}O_3$	5 T	235 K	3.74	159.00	[56]

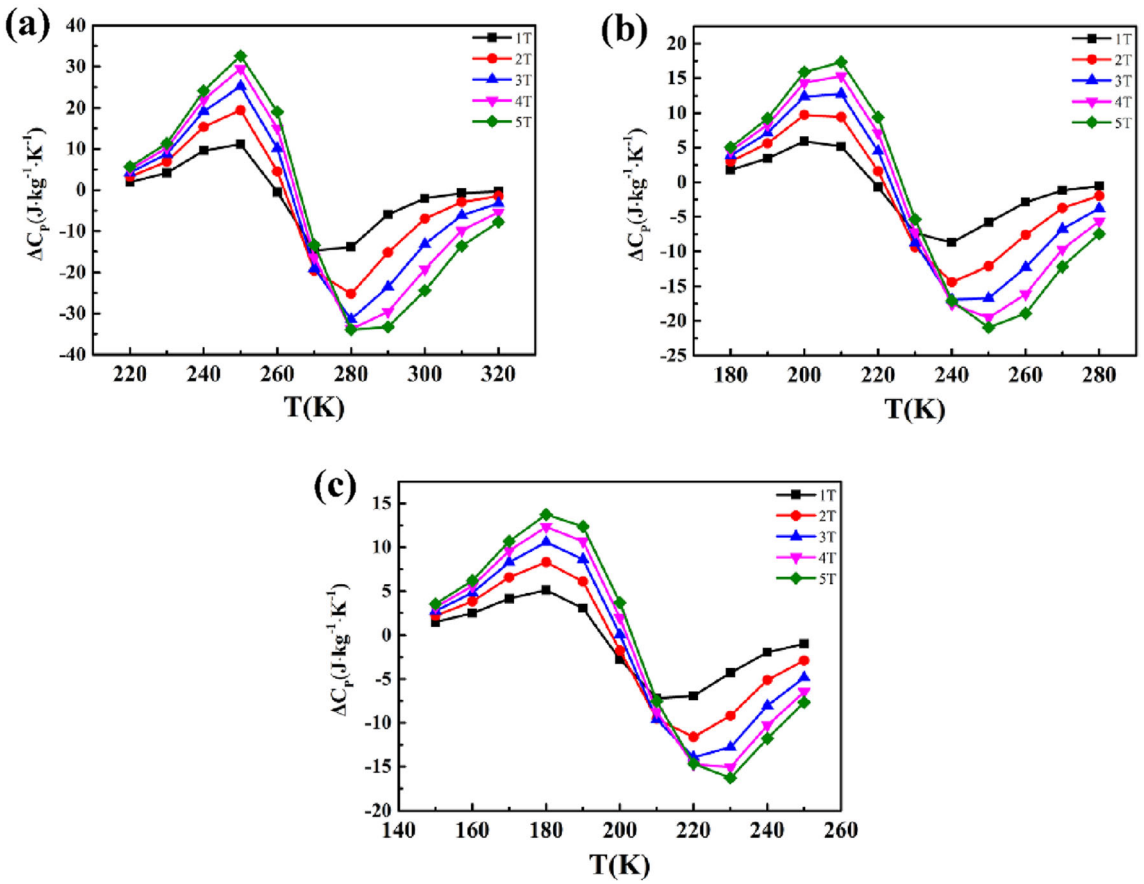

Fig. 15 Variation in the specific heat with T for the $La_{0.8-x}Eu_xCa_{0.1}Sr_{0.1}MnO_3$ (x = 0.05, 0.10, 0.15) in the range of 1–5 T

$$\Delta C_p = C_p(T,\mu_0 H) - C_p(T,0) = T\frac{\partial \Delta S_M^{Max}(T,\mu_0 H)}{\partial T}. \quad (13)$$

Figure 15 demonstrates that the ΔC_p of the LECSMO changes the sign from a positive sign to a negative sign around Tc. As H increases, the magnitude of ΔC_p^{max} as well as ΔC_p^{min} has monotonicity. Since both ΔS_M and dM/dT are considered negative, the situation's total entropy drops during the magnetization process.

4 Conclusion

Polycrystalline powder samples of LECSMO were prepared using the S–G method. The crystal structure, magnetic properties, and magnetocaloric effect of LECSMO were investigated. XRD analysis showed that LECSMO is a rhombohedral perovskite structure in the Pbnm space group. Scanning electron microscope observed an irregular ellipsoidal distribution of LECSMO particles. Magnetic measurements demonstrated that the PM–FM transition occurs near Tc and that Tc reduces as the amount of Eu^{3+} doping rises. Both the method based on the Arrott curve and the normalized curve confirmed that LECSMO undergoes a second-order phase transition near Tc. With a progressive addition of Eu^{3+} doping, the $-\Delta S_M^{max}$ of LECSMO is reduced, but the RCP gradually increases.

Author contributions

ZX contributed to conceptualization, datacuration, writing of the original draft, and writing, reviewing, & editing of the manuscript. XJ contributed to data curation,supporting, and writing, reviewing, & editing of the manuscript. WZ contributed to writing, reviewing, & editing of the manuscript and supporting. ZZ contributed to conceptualization, funding acquisition, and writing, reviewing, & editing of the manuscript.

Funding

The funding was provided by the National Natural Science Foundation of China, Grant No. 52162038.

Data availability

The datasets generated during and analyzed during the current study are available from the corresponding author on reasonable request.

Declarations

Conflict of interest The authors have not disclosed any competing interests.

References

1. Z.J. Xie, Z.G. Zou, B.R. He, L.L. Liu, Front. Mater. **8**, 771941 (2021)
2. Z.J. Xie, Z.G. Zou, X.Y. Jiang, W.J. Zhang, B.R. He, X.N. Han, Physica B: Condensed Matter **639**, 413985 (2022)
3. Z.J. Xie, Z.G. Zou, Z. Mao, X.Y. Jiang, W.J. Zhang, J. Mater. Res. Technol. **21**, 2778 (2022)
4. Z.J. Xie, W.J. Zhang, Z.G. Zou, X.Y. Jiang, J. Magn. Magn. Mater. **536**, 170014 (2022)
5. Z.J. Xie, X.Y. Jiang, Z.G. Zou, Eur. Phys. J. Plus. **137**, 1350 (2022)
6. M.-H. Phan, S.-C. Yu, J. Magn. Magn. Mater. **308**, 325 (2007)
7. K.A. Gschneidner Jr., V.K. Pecharsky, Int. J. Refrig. **31**, 945 (2008)
8. I. Rasta, I. Susila, I. Subagia, J. Phys. Conf. Ser. **953**, 012077 (2018)
9. A. Barman, S. Kar-Narayan, D. Mukherjee, Adv. Mater. Interfaces **6**, 190021 (2019)
10. K. Laajimi, F. Ayadi, M. Kchaw, I. Fourati, M. Khlifi, M.H. Gazzah, J. Dhahri, J. Juraszek, Solid. State. Sci. **119**, 106683 (2021)
11. P. Zhang, H.G. Piao, Y.D. Zhang, J.H. Huang, Acta Phys. Sin **70**, (2021)
12. C. Henchiri, L.H. Omari, T. Mnasri, A. Benali, E. Dhahri, M.A. Valente, J. Alloys Compd. **905**, 194196 (2022)
13. J. Meyers, S. Chumbley, W. Choe, G.J. Miller, Phys. Rev. B Condens. **66**, (2002)
14. B. Podmiljsak, I. Skulj, B. Markoli, K.Z. Rozman, P.J. McGuiness, S. Kobe, J. Magn. Magn. Mater. **321**, 300 (2009)
15. V.D. Buchel'nikov, A.N. Vasiliev, V.V. Koledov, S.V. Taskaev, V.V. Khovaylo, V.G. Shavrov, Phya-Usp. **49**, 871 (2006)
16. G. Akça, S. Kılıç Çetin, A. Ekicibil, Ceram. Int. **43**, 15811 (2017)
17. A. Elghoul, A. Krichene, N. Chniba Boudjada, W. Boujelben, Ceram. Int. **44**, 12723 (2018)

18. Z. Liu, W.G. Lin, K.W. Zhou, J.L. Yan, Ceram. Int. **44**, 2797 (2018)
19. A. Selmi, R. Mnassri, W. Cheikhrouhoukoubaa, N. Chniba Boudjada, A. Cheikhrouhou, Ceram. Int. **41**, 7723 (2015)
20. J. Moradi, M.E. Ghazi, M.H. Ehsani, P. Kameli, J. Solid State Chem. **215**, 1 (2014)
21. T. Raoufi, M.H. Ehsani, D.S. Khoshnoud, J. Alloys Compd. **689**, 865 (2016)
22. X. Zhang, J. Fan, L. Xu, D. Hu, W. Zhang, Y. Zhu, Magnetic and magnetocaloric properties of nanocrystalline $La_{0.5}Sr_{0.5}$-MnO3. Ceram **42**, 1476 (2016)
23. G. Kadim, R. Masrour, A. Jabar, E.K. Hlil, Phys. A **573**, 125936 (2021)
24. A. Szewczyk, M. Gutowska, B. Dabrowski, T. Plackowski, N.P. Danilova, Y.P. Gaidukov, Phys. Rev. B **71**, 224423 (2005)
25. M. Jeddi, H. Gharsallah, M. Bekri, E. Dhahri, E.K. Hlil, J. Low Temp. Phys. **198**, 135 (2020)
26. M.-H. Phan, Y. u Hur, NH Appl. Phys. Lett. **86**, 072504 (2005)
27. F. Cao, H. Chen, Z. Xie, Y. Lu, J. Zhao, X. Jin, Chin. J. Phys. **65**, 424–435 (2020)
28. A.B. Hassine, A. Dhahri, M.L. Bouazizi, M. Oumezzine, E.K. Hlil, Ceram. Int. **43**(1), 1390–1393 (2017)
29. S. Vadnala, S. Asthana, J. Magn. Magn. Mater. **446**, 68–79 (2018)
30. H. Chen, C. Li, J. Zhao, Y. Lu, F. Cao, W. Wang, X. Jin, J. Supercond. Nov. Magn. **34**, 2651–2666 (2021)
31. V.M. Goldschmidt, Sci. Nat. **14**, 477 (1926)
32. J.M.M. Medarde, P. Lacorre, S. Rosenkranz, P. Fischer, K. Gobrecht, Phys. Rev. B **52**, 9248 (1995)
33. C. Kursun, M. Gogebakan, E. Uludag, M.S. Bozgeyik, F.S. Uludag, Sci. Rep. **8**, 13083 (2018)
34. Z. Ma, J. Mohapatra, K. Wei, J.P. Liu, S. Sun, Chem. Rev. **123**, 3094 (2023)
35. R.D. Shannon, Acta Crystallogr. Sect. A: Found. Crystallogr. **32**, 751 (1976)
36. P.G. De Gennes, Phys. Rev. **118**, 141 (1960)
37. M. Kochmański, T. Paszkiewicz, S. Wolski, Eur. J. Phys. **34**, 1555 (2013)
38. S. Hcini, M. Boudard, S. Zemni, Appl. Phys. A **115**, 985 (2014)
39. K.H.J. Buschow, F.R. Boer, *Physics of magnetism and magnetic materials introduction, 1st end* (Springer, Boston, 2003), pp.19–42
40. V. Franco, J.S. Blazquez, A. Conde, Appl. Phys. Lett. **89**, 222512 (2006)
41. V. Franco, A. Conde, Int. J. Refrig. **33**, 465 (2010)
42. K.A. Gschneidner, V. Pecharsky, A. Tsokol, Rep. Prog. Phys. **68**, 1479 (2005)
43. M. Földeàki, R. Chahine, T. Bose, J. Appl. Phys. **77**, 3528 (1995)
44. V. Franco, J. Blázquez, B. Ingale, A. Conde, Annu. Rev. Mater. **42**, 305 (2012)
45. P.T. Phong, N.V. Dang, P.H. Nam, L.T.H. Phong, D.H. Manh, N.M. An, I.N. Lee, J. Alloys Compd. **683**, 67–75 (2016)
46. S. Yu Dan' kov, A.M. Tishin, V.K. Pecharsky, K.A. Jr. Gschneidner, Phys. Rev. B **57**, 3478 (1998)
47. V.K. Pecharsky, K.A. Gschneidner, J. Phys. Rev. Lett. **78**, 4494 (1997)
48. M.S. Kim, J.B. Yang, Q. Cai, X.D. Zhou, W.J. James, W.B. Yelon, P.E. Parris, D. Buddhikot, S.K. Malik, Phys. Rev. B **71**, 014433 (2005)
49. X.Y. Luo, H.F. Yang, S.H. Hua, Q. Wu, N.J. Yu, P.Y. Zhang, H.L. Ge, Bull. Mater. **44**, 1 (2021)
50. A. Bouderbala, J. Makni-Chakroun, W. Cheikhrouhou-Koubaa, M. Koubaa, A. Cheikhrouhou, S. Nowak, S. Ammar-Merah, Ceram. Int. **41**, 7337 (2015)
51. A. Dhahri, M. Jemmali, E. Dhahri, M.A. Valente, J. Alloys Compd. **638**, 221 (2015)
52. X. Jin, Y. Lu, Y. Sun, H. Wu, X. Sun, F. Cao, J. Zhao, J. Low Temp. Phys. **195**, 403 (2019)
53. Y. Bitla, S.N. Kaul, L.F. Barquín, J. Gutiérrez, J.M. Barandiarán, A. Pena, New. J. Phys. **12**, 093039 (2010)
54. A. Guedri, S. Mnefgui, S. Hcini, E.K. Hlil, A. Dhahri, J. Solid State Chem. **297**, 122046 (2021)
55. H.E. Sekrafi, A. Ben, N. JaziaKharrat, W. Chniba-Boudjada, Boujelben, Solid. State. Sci. **105**, 106274 (2020)
56. E. Bouzaiene, A.H. Dhahri, J. Dhahri, E.K. Hlil, Inorg. Chem. Commun. **132**, 108824 (2021)
57. Y. Zhang, P.J. Lampen, T.-L. Phan, S.C. Yu, H. Srikanth, M.-H. Phan, J. Appl. Phys. **111**, 063918 (2012)